Geochemistry Geophysics Geosystems G3
AN ELECTRONIC JOURNAL OF THE EARTH SCIENCES
Published by AGU and the Geochemical Society

*Article*
Volume 8, Number 9
21 September 2007
Q09011, doi:10.1029/2007GC001717
ISSN: 1525-2027

Click Here for Full Article

# What do the HIRM and *S*-ratio really measure in environmental magnetism?

**Qingsong Liu and Andrew P. Roberts**
*National Oceanography Centre, University of Southampton, European Way, Southampton SO14 3ZH, UK (liux0272@yahoo.com)*

**José Torrent**
*Departamento de Ciencias y Recursos Agrícolas y Forestales, Universidad de Córdoba, Edificio C4, Campus de Rabanales, E-14071 Córdoba, Spain*

**Chorng-Shern Horng**
*Institute of Earth Sciences, Academia Sinica, P.O. Box 1-55, Nankang, Taipei, Taiwan*

**Juan C. Larrasoaña**
*Institut de Ciències de la Terra "Jaume Almera," CSIC, Lluís Solé i Sabarís s/n, E-08028 Barcelona, Spain*

[1] The "hard" isothermal remanent magnetization (HIRM) and the *S*-ratio are widely used in environmental magnetism to quantify the absolute and relative concentrations, respectively, of antiferromagnetic minerals (hematite and goethite) in mineral mixtures. We demonstrate that synthetic Al-substituted hematite and goethite exhibit a wide range of coercivities, which significantly influences the HIRM and *S*-ratio. These parameters are therefore not necessarily straightforward indicators of the absolute and relative concentrations of hematite/goethite. To circumvent this problem, we propose a new parameter (the *L*-ratio), which is the ratio of two remanences after alternating field (AF) demagnetization of an IRM imparted in a 1 T field with a peak AF of 100 mT and 300 mT: $IRM_{AF@300mT}/IRM_{AF@100mT}$. These parameters are easily measured using modern vibrating sample or alternating gradient magnetometers. Changes in HIRM only reflect changes in the absolute concentration of hematite and/or goethite if the *L*-ratio is relatively constant. Conversely, *L*-ratio fluctuations indicate variable coercivities that possibly reflect changes in the source of hematite/goethite. Corresponding HIRM and *S*-ratio variations should be interpreted with caution in such cases. The *L*-ratio can be determined using equivalent terms depending on available instrumentation and measurement protocols. For example, the HIRM is equivalent to $IRM_{AF@300mT}$. Likewise, 0.5 * (SIRM + $IRM_{-100mT}$), where $IRM_{-100mT}$ represents the remanent magnetization obtained by first saturating the sample in a high field and then applying a back-field of −100 mT, is equivalent to $IRM_{AF@100mT}$. The HIRM/[0.5 * (SIRM + $IRM_{-100mT}$)] ratio is therefore a suitable substitute for the *L*-ratio when measurements are made with a long-core magnetometer. The newly proposed *L*-ratio is straightforward to measure on a wide range of instruments and can provide significant new insights and reduce ambiguities associated with interpretation of two widely used parameters in environmental magnetism, the HIRM and *S*-ratio.

**Components:** 5886 words, 4 figures, 1 table.

**Keywords:** *L*-ratio; hematite; HIRM; *S*-ratio; goethite.

**Index Terms:** 1512 Geomagnetism and Paleomagnetism: Environmental magnetism; 1540 Geomagnetism and Paleomagnetism: Rock and mineral magnetism; 1519 Geomagnetism and Paleomagnetism: Magnetic mineralogy and petrology.

**Received** 12 June 2007; **Revised** 20 June 2007; **Accepted** 3 July 2007; **Published** 21 September 2007.

Liu, Q., A. P. Roberts, J. Torrent, C.-S. Horng, and J. C. Larrasoaña (2007), What do the HIRM and *S*-ratio really measure in environmental magnetism?, *Geochem. Geophys. Geosyst.*, *8*, Q09011, doi:10.1029/2007GC001717.

## 1. Introduction

[2] Hematite ($\alpha$-$Fe_2O_3$) and goethite ($\alpha$-FeOOH) have been the subject of many studies because they are important constituents of soils and sediments. For example, they can adsorb significant amounts of phosphate and other ions, thus affecting water quality and soil fertility [*Barrón et al.*, 1988; *Schwertmann*, 1988; *Colombo et al.*, 1994]. They are also important carriers of natural remanent magnetization in rocks and sediments [e.g., *Stokking and Tauxe*, 1990]. Moreover, the presence and preservation of hematite and goethite in soils and sediments are related to environment, so these minerals can provide a variety of environmental magnetic signatures [*Thompson and Oldfield*, 1986; *Verosub and Roberts*, 1995; *Evans and Heller*, 2003]. The concentration of goethite and hematite in soil/loess samples can be semi-quantitatively determined by different methods, such as X-ray powder diffraction, Mössbauer spectroscopy and diffuse reflectance spectroscopy [*Scheinost et al.*, 1998]. Rock magnetic methods can also provide powerful tools for analysis of natural samples because they are rapidly applied, efficient, and highly sensitive. The "hard" isothermal remanent magnetization (HIRM) is commonly used to estimate the absolute concentration of hematite and/or goethite in mineral mixtures that also contain magnetite/maghemite. The HIRM is defined as $0.5 \times (\mathrm{SIRM} + \mathrm{IRM}_{-300\mathrm{mT}})$, where $\mathrm{IRM}_{-300\mathrm{mT}}$ represents the remanent magnetization obtained by first saturating the sample in a high field (e.g., 1 or 1.5 T), and then applying a back-field of −300 mT to reverse the saturation isothermal remanent magnetization (SIRM) contributed by magnetite/maghemite. Theoretically, the HIRM eliminates contributions from the strongly magnetic but low-coercivity ferrimagnetic minerals because they magnetically saturate at fields below 300 mT. The HIRM therefore reflects the magnetic signal carried by the weakly magnetic but high-coercivity antiferromagnetic minerals [*Robinson*, 1986; *Thompson and Oldfield*, 1986]. Relative abundance variations of ferrimagnetic and antiferromagnetic minerals are commonly quantified using the *S*-ratio, which is given by $-\mathrm{IRM}_{-300\mathrm{mT}}/\mathrm{SIRM}$. When the *S*-ratio approaches unity, low-coercivity minerals, such as magnetite and maghemite, are interpreted to magnetically dominate samples. In contrast, when the *S*-ratio is close to zero or if it has negative values, contributions from hematite and/or goethite will be significant. The HIRM and/or the *S*-ratio have been successfully used as proxies for variations in hematite/goethite-bearing eolian dust input into the North Pacific Ocean [*Yamazaki and Ioka*, 1997], the Atlantic Ocean [*Maher and Dennis*, 2001], and the Mediterranean Sea [*Larrasoaña et al.*, 2003a].

[3] Despite widespread use of these parameters in environmental magnetism, interpretation of HIRM and *S*-ratio is not straightforward. *Liu et al.* [2002] pointed out that HIRM can be problematic when the remanence carried by hematite/goethite is completely masked by a strongly magnetic background signal because the HIRM can have similar magnitude to the measurement errors. The basic assumption underlying the use of HIRM is that hematite and goethite both have a saturation field >300 mT [e.g., *Dankers*, 1981], and contributions from magnetite and maghemite are therefore cancelled when calculating HIRM. However, the magnetic properties of hematite and goethite are controlled by both grain size [*Dekkers*, 1989; *de Boer and Dekkers*, 1998] and isomorphic cation substitutions [*Mathé et al.*, 1999; *Wells et al.*, 1999; *Liu et al.*, 2004]. We demonstrate in this study that the coercivities of aluminous hematite and goethite range widely, as do the corresponding HIRM and *S*-ratio values. We systematically investigated a set of hydrothermally synthesized fine-grained aluminous hematite and goethite samples to elucidate the mechanisms that cause large variations in the HIRM and *S*-ratio of these two minerals. We then propose a new parameter to determine whether samples contain hematite and goethite with variable coercivities in mixtures with strongly magnetic minerals. Finally, two case studies are presented to further illustrate the usefulness of these magnetic parameters in interpretation of environmental changes.

## 2. Samples and Methods

[4] We analyzed samples of synthetic Al-hematite [*Barrón et al.*, 1988; *Colombo et al.*, 1994; *Roberts*

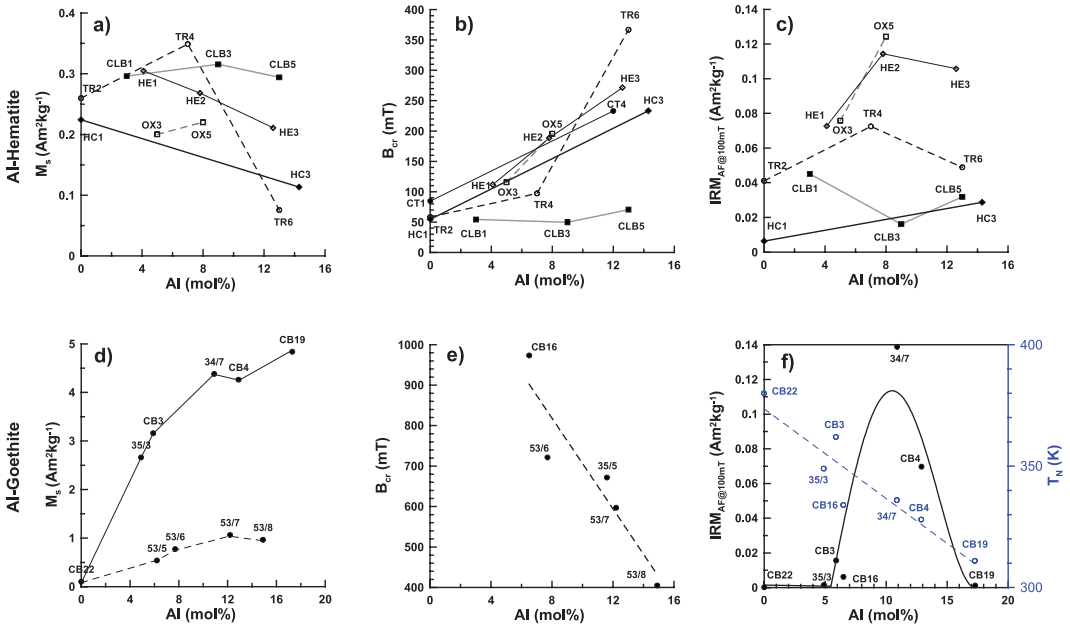


**Figure 1.** Magnetic properties of different (a–c) Al-hematite and (d–f) Al-goethite samples: (a and d) $M_s$, (b and e) $B_{cr}$, and (c and f) $IRM_{100mT}$, all versus mol% Al. In Figure 1f the $T_N$ of Al-goethite samples (open circles) is also presented (data from *Liu et al.* [2004]). The dashed line is the linear trend between $T_N$ and Al content. Data in Figure 1d represent $M_{5T}$ rather than $M_s$ and were measured at 20 K to avoid effects of $T_N$, while those in Figures 1a–1c, 1e, and 1f were measured at room temperature.

*et al.*, 2006] and Al-goethite [*Schulze and Schwertmann*, 1984, 1987; *Torrent et al.*, 1987; *Liu et al.*, 2004] with a wide range of Al mol% (Figure 1) and crystal properties. The synthesis procedures and main physical and magnetic properties of these samples are described by *Barrón et al.* [1988], *Colombo et al.* [1994], *Liu et al.* [2004], and *Roberts et al.* [2006] (see also Table 1). These samples are useful for understanding natural environments because they have Al contents (Figure 1) within the range found in soils [*Torrent et al.*, 1980].

[5] Hematite/goethite powders (~10 mg mass) were prepared by dispersing them in a $CaF_2$ matrix. The room-temperature magnetic hysteresis loops of hematite/goethite samples were measured using a Princeton Measurements Corporation vibrating sample magnetometer (VSM, maximum applied field = 1 T). Hysteresis parameters (saturation magnetization, $M_s$; and saturation remanence, $M_{rs}$; coercive force, $B_c$) were obtained after correcting the high-field slope. To obtain the coercivity of remanence ($B_{cr}$), samples were remagnetized from +1 T using backfields up to −1 T. Alternating field (AF) demagnetization of the IRM imparted in the 1 T field was also performed using the VSM. The decay rate of the AF is 2% per cycle. Hereafter, the residual remanence after AF demagnetization is denoted as $IRM_{AF@xmT}$, where x mT is the peak AF. The Néel temperature ($T_N$) of Al-goethite samples is <400 K, therefore $M_s$ is controlled not only directly by the Al content, but also by associated changes in $T_N$ with respect to the Al content. To minimize the latter effects and to highlight the Al-dependence of $M_s$, hysteresis loops of the Al-goethite samples were analyzed again at 20 K using a Quantum Designs Magnetic Properties Measurement System (MPMS). The saturation field was 5 T, but it should be noted that even such a high field cannot magnetically saturate goethite [*Rochette et al.*, 2005]. Therefore the hysteresis loops measured for the Al-goethite samples are only minor loops and the magnetization at 5 T is named $M_{5T}$ rather than $M_s$.

## 3. Magnetic Properties of the Studied Al-Hematite and Al-Goethite Samples

### 3.1. Magnetic Properties of Al-Hematite

[6] The Al-dependence of the magnetic properties for the studied Al-hematite and Al-goethite samples is shown in Figure 1. For the two pure hematite samples (Al mol% = 0), $M_s$ ranged between ~0.22 and ~0.26 $Am^2\ kg^{-1}$ (Figure 1a), which is consistent with previous studies [*Dunlop*

**Table 1.** Methods Used to Synthesize the Studied Hematite and Goethite Samples

| Mineral | Sample | Al mol% | Procedure and Solutions Used | Alkali Added | Final [OH] or pH | Reference |
|---|---|---|---|---|---|---|
| Hematite | CB22 | 0 | 200 mL 0.5 *M* $Fe(NO_3)_3$ | 2 *M* KOH | 0.9–1.35 | *Torrent et al.* [1990] |
| | 35/3 | 4.9 | 1.5 L 0.5 *M* $Al(NO_3)_3$ + 900 mL 5 *M* KOH + 225 mL 1 *M* $Fe(NO_3)_3$ for 1310 days at 25°C | 5 *M* KOH | ~12 | *Schulze and Schwertmann* [1987] |
| | CB3 | 5.9 | 100 mL 1 *M* $Fe(NO_3)_3$ + 0 to 75 mL 0.5 *M* $Al(NO_3)_3$ at 323°C | 5 *M* KOH | 0.6–1.2 | *Torrent et al.* [1990] |
| | CB16 | 6.5 | 100 mL 1 *M* $Fe(NO_3)_3$ + 0 to 75 mL 0.5 *M* $Al(NO_3)_3$ | 3 *M* KOH | 0.6–1.35 | *Torrent et al.* [1990] |
| | 53/6 | 7.7 | solutions of $Al(NO_3)_3$, $Fe(NO_3)_3$, and KOH. Detailed procedure not recorded | KOH | ~12 | - |
| | 34/7 | 10.9 | mixtures of $Fe(NO3)_3$ and $AlCl_3$ solutions stored for 14 days at 70°C | 0.3 M KOH | ~12 | *Schulze and Schwertmann* [1987] |
| | 35/5 | 11.6 | 1.5 L 0.5 *M* $Al(NO_3)_3$ + 900 mL 5 *M* KOH + 225 mL 1 *M* $Fe(NO_3)_3$ for 1310 days at 25°C | 5 *M* KOH | ~12 | *Schulze and Schwertmann* [1987] |
| | 53/7 | 12.2 | solutions of $Al(NO_3)_3$, $Fe(NO_3)_3$, and KOH | KOH | ~12 | - |
| | CB4 | 12.9 | 100 mL 1 *M* $Fe(NO_3)_3$ + 0 to 75 mL 0.5 *M* $Al(NO_3)_3$ at 298°C | 5 *M* KOH | 0.6–1.2 | *Torrent et al.* [1990] |
| | 53/8 | 14.9 | solutions of $Al(NO_3)_3$, $Fe(NO_3)_3$, and KOH | KOH | ~12 | - |
| | CB19 | 17.3 | 100 mL 1 *M* $Fe(NO_3)_3$ + 0 to 75 mL 0.5 *M* $Al(NO_3)_3$ | 3 *M* KOH | 0.6–1.35 | *Torrent et al.* [1990] |
| Goethite | CT1 | 0.0 | solutions of $Fe(NO_3)_3$ + $Al(NO_3)_3$ | KOH | 9.5 | *Colombo et al.* [1994][a] |
| | HC1 | 0.0 | solutions of $Fe(NO_3)_3$ + $Al(NO_3)_3$ | KOH | 8.0 | *Barrón et al.* [1988][b] |
| | TR2 | 0.0 | solutions of $Fe(NO_3)_3$ + $Al(NO_3)_3$ | KOH | 9.0 | *Colombo et al.* [1994] |
| | OX1 | 0.0 | solutions of $Fe(NO_3)_3$ + $Al(NO_3)_3$ | KOH | 5.0 | *Colombo et al.* [1994] |
| | CLB1 | 3.0 | solutions of $Fe(NO_3)_3$ + $Al(NO_3)_3$ | KOH | 5.5 | *Colombo et al.* [1994][a] |
| | HE1 | 4.1 | solutions of $Fe(NO_3)_3$ + $Al(NO_3)_3$ | KOH | | *Barrón et al.* [1988][b] |
| | OX3 | 5.0 | solutions of $Fe(NO_3)_3$ + $Al(NO_3)_3$ | KOH | 6.0 | *Colombo et al.* [1994] |
| | TR4 | 7.0 | solutions of $Fe(NO_3)_3$ + $Al(NO_3)_3$ | KOH | 8.0 | *Colombo et al.* [1994] |
| | HC2 | 7.5 | solutions of $Fe(NO_3)_3$ + $Al(NO_3)_3$ | KOH | 8.0 | *Barrón et al.* [1988][b] |
| | HE2 | 7.8 | solutions of $Fe(NO_3)_3$ + $Al(NO_3)_3$ | KOH | | *Barrón et al.* [1988][b] |
| | OX5 | 8.0 | solutions of $Fe(NO_3)_3$ + $Al(NO_3)_3$ | KOH | 6.5 | *Colombo et al.* [1994] |
| | CLB3 | 9.0 | solutions of $Fe(NO_3)_3$ + $Al(NO_3)_3$ | KOH | 6.0 | *Colombo et al.* [1994][a] |
| | HC4 | 10.2 | solutions of $Fe(NO_3)_3$ + $Al(NO_3)_3$ | KOH | | *Barrón et al.* [1988][b] |
| | CT4 | 12.0 | solutions of $Fe(NO_3)_3$ + $Al(NO_3)_3$ | KOH | 10 | *Colombo et al.* [1994][a] |
| | HE3 | 12.6 | solutions of $Fe(NO_3)_3$ + $Al(NO_3)_3$ | KOH | | *Barrón et al.* [1988][b] |
| | CLB5 | 13.0 | solutions of $Fe(NO_3)_3$ + $Al(NO_3)_3$ | KOH | 6.5 | *Colombo et al.* [1994][a] |
| | TR6 | 13.0 | solutions of $Fe(NO_3)_3$ + $Al(NO_3)_3$ | KOH | 9.0 | *Colombo et al.* [1994] |
| | HC3 | 14.2 | solutions of $Fe(NO_3)_3$ + $Al(NO_3)_3$ | KOH | | *Barrón et al.* [1988][b] |

[a] Samples were named without the "CL" prefix in this paper.
[b] Samples were named without the "H" prefix in this paper.

*and Özdemir*, 1997]. For the whole set of samples, there is no straightforward relationship between $M_s$ and Al mol% (Figure 1a). This observation is explained below.

[7] Within the basal plane of the hematite structure (space group $R\bar{3}c$), the two adjacent Fe layers are arranged with opposite spin directions. The overall magnetization is therefore antiferromagnetic. Upon cooling, hematite undergoes a spin-flip transition at the Morin temperature, $T_M$ (~236 K for pure hematite). Above $T_M$, the magnetically ordered spins lie in the basal plane. When the applied field

is parallel to the basal plane, the two groups of antiferromagnetic sublattice moments orient themselves almost perpendicular to the field direction but with a small angle between two sublattice moments, which results in a net canted antiferromagnetism along the field direction. The existence of vacancies or impurities in the crystal lattice will also produce unbalanced sublattice moments within the basal plane for hematite. With increasing Al mol%, the imbalance in the sublattice moments will increase, resulting in an increase in the bulk $M_s$. However, at a critical Al content, dilution effects resulting from increasing Al versus Fe contents gradually become dominant, and $M_s$ will begin to decrease. This pattern is supported by the trends for the TR, CLB and OX sample series in Figure 1a. The coercivity of Al-hematite is dominantly controlled by internal stress, which increases with increasing Al content. For the respective sample series, which were produced using different synthesis methods, a clear trend toward higher coercivities is observed with higher Al substitution (Figure 1b). However, for similar Al contents, coercivities vary significantly among different sample series due to non-uniformity of Al substitutions within the crystal lattice. For natural samples, the bulk remanence often consists of contributions from both antiferromagnetic and strongly ferrimagnetic minerals (e.g., magnetite and maghemite). To eliminate contributions from strongly ferrimagnetic minerals such as magnetite, $SIRM_{AF@100mT}$ is used to enhance the antiferromagnetic contributions (Figure 1c).

### 3.2. Magnetic Properties of Al-Goethite

[8] Al-goethite has more complicated magnetic behavior than Al-hematite (Figures 1d–1f). Goethite has uniaxial antiferromagnetism ($T_N \sim 395–400$ K) [*Özdemir and Dunlop*, 1996], in which the spins for the two sublattices couple along the crystallographic *c*-axis [*Forsyth et al.*, 1968]. Unlike the canting mechanism for remanences carried by hematite, the antiferromagnetism of goethite is unbalanced by different numbers of spins in the two sublattices (A or B) due to the presence of defects and/or isomorphous cation substitutions in the crystal lattice [*Özdemir and Dunlop*, 1996]. Generally, with increasing Al-substitution (up to 10–15 mol%), Al ions preferentially cluster along the same sub-lattice where the earlier substitutions of Al ions occurred [*Pollard et al.*, 1991], thus the bulk $M_s$ due to the unbalanced moments steadily increases with increasing Al content (Figure 1d).

[9] Goethite has a $T_N$ just above room temperature; therefore slight changes in $T_N$ due to Al substitution can significantly affect the room-temperature $M_s$. However, this problem can be avoided if $M_s$ is measured at 20 K. Similar to the Al-hematite samples, due to non-uniformity of Al substitution, the $M_{5T}$ values of the Al-goethite samples fall on two major trends. The "53" sample series has much lower $M_{5T}$ values than the other samples. Nevertheless, it is clear that $M_{5T}$ increases with increasing Al mol% (Figure 1d). $B_{cr}$ decreases almost linearly with increasing Al mol% because of the dominant effect of $T_N$ on the room-temperature magnetic properties of Al-goethite (Figure 1e). For Al-goethite, $IRM_{AF@100mT}$ has low values for Al mol% $<\sim$5 mol% (Figure 1f); it then increases by at least an order of magnitude when Al content increases to about 12 mol%. After that, $IRM_{AF@100mT}$ decreases again due to the effects of thermal agitation as $T_N$ gradually approaches room temperature with increasing Al substitution (Figure 1f). Therefore only goethite with intermediate Al content ($\sim$5–12 mol%) has $IRM_{AF@100mT}$ values comparable to Al-hematite that can therefore significantly contribute to the bulk sedimentary remanence.

## 4. *S*-Ratio and HIRM Behavior and a New Parameter, the *L*-Ratio

[10] The $B_{cr}$ values of the studied Al-goethite samples are >300 mT, which will produce negative *S*-ratio values (Figure 2a). However, this will rarely be the case with natural samples because of contributions to the bulk remanence from other magnetic minerals with lower $B_{cr}$ values. For the studied Al-hematite samples, the *S*-ratio usually ranges between 0 and 1, depending on the corresponding $B_{cr}$ values (Figure 2a). Substantial variations in coercivity of Al-hematite make it unwise to use the *S*-ratio alone for quantifying the relative contributions of magnetite and hematite in natural samples. HIRM has been widely interpreted as a proxy for the absolute concentration of antiferromagnetic minerals in samples. However, as shown in Figure 2b, HIRM values for Al-hematite are controlled by its coercivity. Therefore HIRM cannot be used alone as a proxy for the absolute concentration of antiferromagnetic minerals if the coercivity values of the antiferromagnetic minerals are unknown. Magnetic signals carried by antiferromagnetic minerals are often masked by the strongly magnetic background due to the presence of magnetite and maghemite, therefore it is not

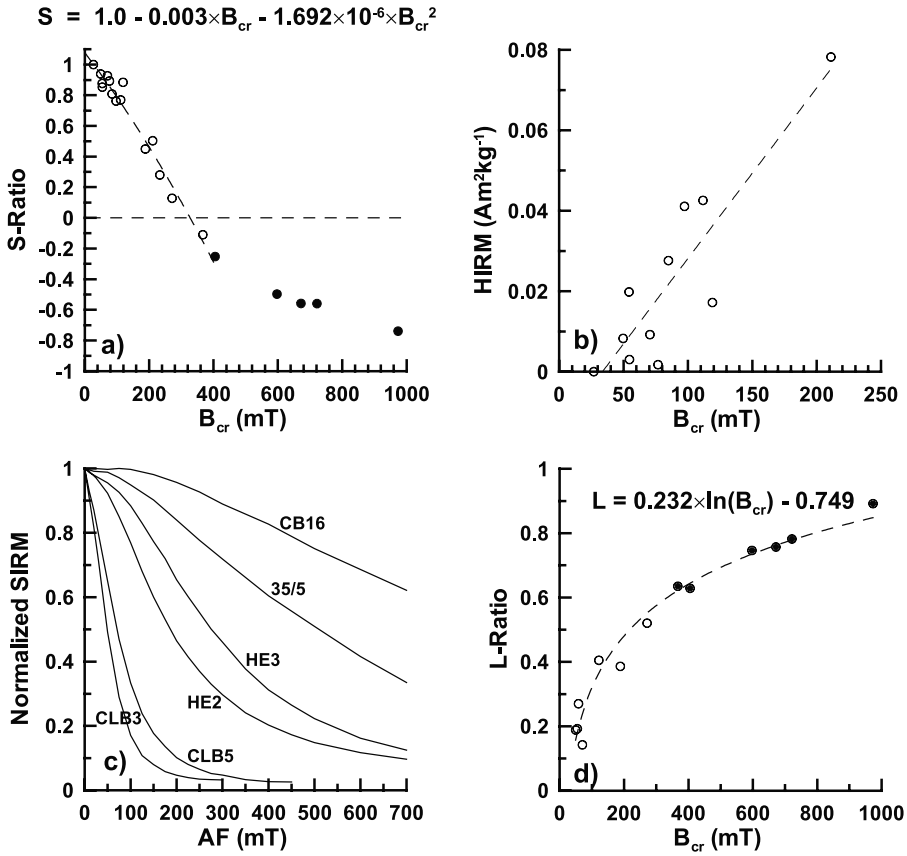


**Figure 2.** (a) *S*-ratio and (b) HIRM against $B_{cr}$ for the studied hematite (open circles) and goethite samples (solid circles). The dashed curve in Figure 2a indicates a second-order polynomial trend, and the dashed line in Figure 2b is a linear trend for hematite samples. In Figure 2b, only the data for samples with $M_{rs}/M_s > 0.5$ are used to avoid the effects of significant superparamagnetic behavior in samples. HIRM carried by goethite does not follow this trend because its remanence is not a linear function of Al content. (c) AF demagnetization spectra for selected Al-hematite and Al-goethite samples (see Figure 1 for other properties of the same samples). (d) Correlation between the *L*-ratio and $B_{cr}$ for the studied Al-hemat ite and Al-goethite samples (the dashed curve in Figure 2d is a power law fit).

easy to directly determine the coercivity values of these antiferromagnetic minerals in natural samples by traditional methods.

[11] In order to determine cases where the HIRM and *S*-ratio might continue to be useful in environmental magnetic studies, we propose a new parameter, the *L*-ratio, which is defined as $IRM_{AF@HmT}/IRM_{AF@LmT}$, where the subscripts HmT and LmT denote the high and low peak AF (units are in mT), respectively. In this study, we used 300 and 100 mT for HmT and LmT, respectively. The *L*-ratio enables semi-quantitative identification of the presence of $B_{cr}$ variations in samples, which would clarify the interpretation of HIRM and *S*-ratio, even in the presence of a strong ferrimagnetic background signal. The remanence carried by strongly ferrimagnetic minerals can be generally removed by AF demagnetization at 100 mT. Thus variations in the *L*-ratio will dominantly reflect the relative $B_{cr}$ distribution of the constituent antiferromagnetic minerals within a suite of samples. The gradual decay of remanence upon AF demagnetization for all of the studied samples indicates a continuous coercivity distribution (Figure 2c). However, samples with higher $B_{cr}$ values are more resistant to the maximum AF. Thus, with increasing $B_{cr}$, the *L*-ratio gradually approaches 1 (Figure 2d). The *L*-ratio is useful for constraining interpretation of HIRM and *S*-ratio values. In cases where the *L*-ratio is constant for a suite of samples, HIRM and *S*-ratio can be safely interpreted in the traditional way. The *L*-ratio is useful when hematite is the major antiferromagnetic phase in samples. In contrast, when goethite has a significant influence on the bulk remanence, interpretation of the *L*-ratio is less straightforward because the relationship between $B_{cr}$ and remanence is non-linear with respect to Al mol%

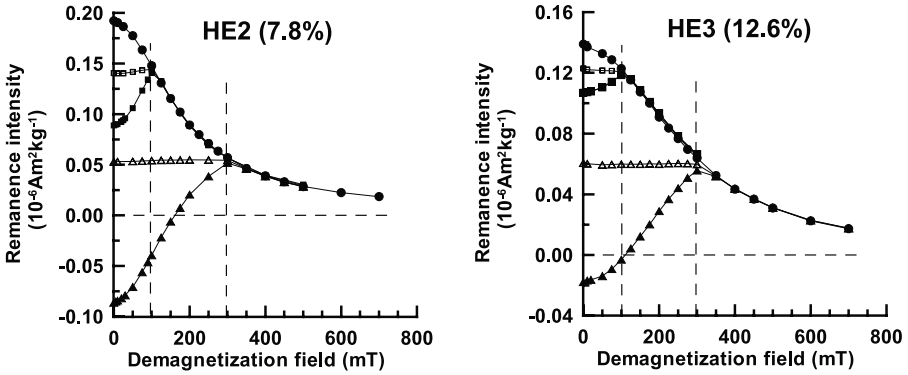


**Figure 3.** AF demagnetization spectra of IRM (solid circles), $IRM_{-300mT}$ (solid triangles), and the calculated HIRM (open triangles), $IRM_{-100mT}$ (solid rectangles), and the calculated 0.5 * (SIRM + $IRM_{-100mT}$) (open rectangles) for Al-hematite samples HE2 (Al = 7.8 mol%) and HE3 (Al = 12.6 mol%). The HIRM values were calculated after each AF demagnetization step. The vertical dashed lines indicate the value of $IRM_{AF@100mT}$ and $IRM_{AF@300mT}$. The data demonstrate that the HIRM and 0.5 * (SIRM + $IRM_{-100mT}$) values are comparable to $IRM_{AF@300mT}$ and $IRM_{AF@100mT}$, respectively. This indicates that the *L*-ratio can be equivalently determined using different parameters depending on the available instrumentation and measurement protocols adopted.

(Figures 1e and 1f). If the Al content is constant, then interpretation of the *L*-ratio in goethite-bearing samples can be straightforward.

[12] The *L*-ratio defined above can be easily measured for discrete samples with an automated VSM. For continuous u-channel sample measurement [*Weeks et al.*, 1993], the maximum applied AF is generally <150 mT. However, in practice, as demonstrated in Figure 3, HIRM is equivalent to $IRM_{AF@300mT}$. Furthermore, 0.5 * (SIRM + $IRM_{-100mT}$), where $IRM_{-100mT}$ represents the remanent magnetization obtained by first saturating the sample in a high field and then applying a backfield of −100 mT, is equivalent to $IRM_{AF@100mT}$. The HIRM/(0.5 * (SIRM + $IRM_{-100mT}$) ratio is therefore a suitable substitute for measurements made with a long-core magnetometer.

## 5. Case Studies

[13] To examine the usefulness of the *L*-ratio, two case studies are illustrated in Figure 4. The first deals with long-term paleoclimatic changes recorded in sediments (between 75.46 revised meters composite depth (rmcd) and 87.23 rmcd, corresponding to ~2.4–2.9 Ma) from ODP Site 967 from the eastern Mediterranean Sea [*Larrasoaña et al.*, 2003a]. The magnetic measurements were made at 1-cm intervals. Detailed rock magnetic results demonstrate that hematite is the dominant magnetic mineral responsible for the high coercivity magnetic signal. The *L*-ratio (defined as HIRM/$IRM_{AF@120mT}$) is almost independent of HIRM for this data set (Figure 4a), as indicated by the fact that most of the data fall within a narrow shaded area with reasonably constant *L*-ratio. This suggests that the HIRM changes are dominantly controlled by fluctuations in the concentration of hematite. *Larrasoaña et al.* [2003a] concluded that the hematite particles in the studied eastern Mediterranean sediments originated dominantly from a single source in the northeastern Sahara desert. Nevertheless, a correlation between the *L*-ratio and HIRM is observed for some of the data, which reveals a secondary linear trend (Figure 4a). Stratigraphic intervals in which the *L*-ratio is most variable are restricted to organic-rich sapropels where magnetic minerals have undergone diagenetic dissolution [*Larrasoaña et al.*, 2003b]. The data in Figure 4a confirm the interpretation of *Larrasoaña et al.* [2003a] that diagenesis has not significantly influenced the hematite signal in sediments between the sapropel layers for the studied interval of ODP Site 967. In contrast, large changes in the *L*-ratio within the sapropel layers indicate significant fluctuations in the coercivities of hematite particles, which might have been caused by diagenetic dissolution of some of the eolian hematite.

[14] The second case study deals with the HIRM record for a sediment core from the western Philippine Sea [*Horng et al.*, 2003], which received eolian input dominantly from China, but also from other sources, e.g., possibly southern Asia and Australia [*Stancin et al.*, 2006]. The studied inter-

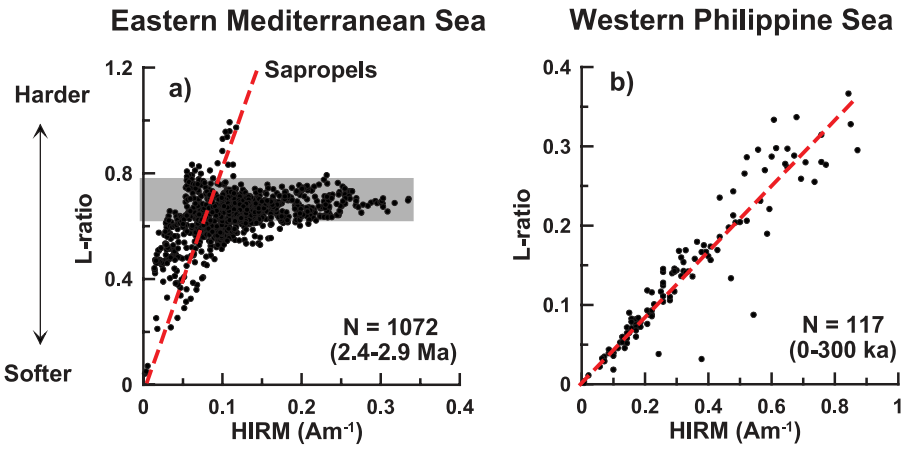


**Figure 4.** Correlations between the *L*-ratio and HIRM for samples from (a) ODP Site 967 from the eastern Mediterranean Sea [*Larrasoaña et al.*, 2003a] and (b) core MD972143 from the western Philippine Sea [*Horng et al.*, 2003]. In Figures 4a and 4b the HIRM values for samples along the linear trends are controlled by variations in coercivity distribution rather than by changes in concentration of hematite and/or goethite. The gray shaded area in Figure 4a indicates a subset of data for which HIRM and *L*-ratio are not correlated. The stable *L*-ratio indicates that variations in HIRM are dominantly caused by changes in the concentration of hematite. In contrast, the correlation between the *L*-ratio and HIRM in Figure 4b indicates that variations in the HIRM are caused by variations in the coercivity of hematite and/or goethite. In such cases, HIRM cannot be used for traditional purposes. Nevertheless, large fluctuations in the *L*-ratio could be sensitive indicators of changes in eolian source. The arrow beside Figure 4a indicates that a higher *L*-ratio value corresponds to magnetically harder minerals. N indicates the total number of data points shown in each plot.

val is the uppermost 8.89 m of the core (~300 ka) with an average sampling rate of ~7.6 cm. The *L*-ratio and HIRM have an excellent linear correlation, which indicates that the observed HIRM changes are controlled by changes in the coercivity distribution rather than by the concentration of the antiferromagnetic minerals (Figure 4b). This is a clear case where parameters such as the HIRM and *S*-ratio do not provide useful quantitative information about variations in the absolute or relative concentration of antiferromagnetic minerals. Nevertheless, identification of variations in the *L*-ratio is useful because it probably indicates variability in eolian sources. Comparison of absolute *L*-ratio values for the eastern Mediterranean Sea with those from the western Philippine Sea is also useful because it indicates that the hematite particles that originated from the northeastern Sahara desert are magnetically harder than those derived from eastern Asia.

## 6. Further Evaluations of the *L*-Ratio

[15] Coercivity spectra of magnetic minerals are related to magnetic mineralogy, grain size, and other factors (non-stoichiometry, defect density, etc). Different minerals and size fractions will therefore have overlapping coercivity spectra. Unmixing algorithms [e.g., *Egli*, 2004] or first-order reversal curve diagrams [e.g., *Roberts et al.*, 2006] can be used to isolate different magnetic components, but application of these methods to large numbers of samples is not usually feasible because they require detailed and time-consuming measurements. Rough-cut parameters such as the HIRM and *S*-ratio are therefore widely used. In these parameters, the IRM is divided into three fractions, which are conventionally referred to as the soft ($M_{soft}$, <100 mT), intermediate ($M_{intermediate}$, 100–300 mT) and hard ($M_{hard}$, >300 mT) components. The newly proposed *L*-ratio uses the same strategy to aid interpretation of these widely used parameters. Simplistic interpretations of these parameters often ignore the fact that the three remanence fractions cannot be strictly translated into clearly demarcated mineral components or size fractions. The intermediate fraction and even the soft fraction may originate mainly in "hard" carriers like hematite, as shown in this paper. Similarly, the intermediate and hard fractions can also contain significant or even dominant contributions from "soft" ferrimagnets, as shown by *Liu et al.* [2002]. Ambiguities resulting from coercivity overlaps [e.g., *Roberts et al.*, 2006] in mixed mineral

assemblages can often be efficiently removed using a range of thermomagnetic techniques [e.g., *Larrasoaña et al.*, 2003a]. Remaining ambiguities can be resolved using auxiliary rock magnetic and other analyses [e.g., *Evans and Heller*, 2003].

[16] The *L*-ratio is therefore another way of using standard measurements to compare the three coercivity fractions (*L*-ratio = $M_{hard}/[M_{hard} + M_{intermediate}]$) that control the *S*-ratio and HIRM to enable more rigorous interpretation of these parameters. Once it is demonstrated that $M_{intermediate}$ and $M_{hard}$ are carried by hematite, using constraints from thermomagnetic and other analyses, it can be concluded that variations in the *L*-ratio reflect changes in the coercivity of hematite. As we have demonstrated above, coercivity variations reflect an intrinsic property of hematite that is associated with stoichiometry, defect density and/or grain size, which will be closely related to the environment in which the hematite formed. Variations in the *L*-ratio can therefore provide a means to detect the possibility of variable hematite provenance in a sedimentary sequence.

[17] In summary, the *L*-ratio provides useful constraints to enable correct interpretation of the *S*-ratio and HIRM without involving a large amount of extra work. Additionally, it has the potential to enable monitoring of changes in hematite provenance, as demonstrated in the case studies outlined above.

## 7. Conclusions

[18] Large changes in the coercivity of hematite and goethite grains in mineral assemblages with different origins mean that HIRM and *S*-ratio alone cannot be simply interpreted in terms of the absolute and relative changes, respectively, in the concentration of antiferromagnetic minerals. However, this problem can be partially circumvented by using a new parameter, the *L*-ratio, which is defined as the ratio of two residual remanences after AF demagnetization of an IRM imparted in a 1 T field with a peak AF at 100 mT and 300 mT ($IRM_{AF@300mT}/IRM_{AF@100mT}$). The HIRM only represents absolute changes in the concentration of antiferromagnetic minerals when the *L*-ratio is relatively constant. Large fluctuations in the *L*-ratio point to significant changes in the coercivity of antiferromagnetic minerals, which, in turn, implies variations in sediment provenance. The *L*-ratio is therefore an important new parameter in environmental magnetism because it provides crucial ground-truthing for the long-used HIRM and *S*-ratio parameters, as well as providing information concerning potential variations in provenance of antiferromagnetic minerals.

## Acknowledgments

[19] Q. S. Liu was supported by the European Commission through a Marie-Curie Fellowship (IIF), proposal 7555. The contribution of J. Torrent was supported by the Spanish Ministerio de Ciencia y Tecnoloğacute;a, project AGL2003-01510. J. C. Larrasoaña benefits from a "Ramón y Cajal" contract of the Ministerio de Educación y Ciencia. This paper was improved as a result of insightful comments from anonymous journal reviewers and Associate Editor Michael Jackson.

## References

Barrón, V., M. Herruzo, and J. Torrent (1988), Phosphate adsorption by aluminous hematites of different shapes, *Soil Sci. Soc. Am. J.*, *52*, 647–651.

Colombo, C., V. Barrón, and J. Torrent (1994), Phosphate adsorption and desorption in relation to morphology and crystal properties of synthetic hematites, *Geochim. Cosmochim. Acta*, *58*, 1261–1269.

Dankers, P. (1981), Relationship between median destructive field and remanent coercive forces for dispersed natural magnetite, titanomagnetite and hematite, *Geophys. J. R. Astron. Soc.*, *64*, 447–461.

de Boer, C. B., and M. J. Dekkers (1998), Thermomagnetic behaviour of haematite and goethite as a function of grain size in various non-saturating magnetic fields, *Geophys. J. Int.*, *133*, 541–552.

Dekkers, M. J. (1989), Magnetic properties of natural goethite - I. Grain-size dependence of some low- and high-field related rock magnetic parameters measured at room temperature, *Geophys. J.*, *97*, 323–340.

Dunlop, D. J., and Ö. Özdemir (1997), *Rock Magnetism: Fundamentals and Frontiers*, Cambridge Univ. Press, Cambridge, U. K.

Egli, R. (2004), Characterization of individual rock magnetic components by analysis of remanence curves, 1. Unmixing natural sediments, *Stud. Geophys. Geod.*, *48*, 391–446.

Evans, M. E., and F. Heller (2003), *Environmental Magnetism: Principles and Applications of Enviromagnetics*, Academic, San Diego, Calif.

Forsyth, J. B., I. G. Hedley, and C. E. Johnson (1968), The magnetic structure and hyperfine field of goethite ($\alpha$-FeOOH), *J. Phys. C*, *1*, 179–188.

Horng, C.-S., A. P. Roberts, and W.-T. Liang (2003), A 2.14-Myr astronomically tuned record of relative geomagnetic paleointensity from the western Philippine Sea, *J. Geophys. Res.*, *108*(B1), 2059, doi:10.1029/2001JB001698.

Larrasoaña, J. C., A. P. Roberts, E. J. Rohling, M. Winklhofer, and R. Wehausen (2003a), Three million years of monsoon variability over the northern Sahara, *Clim. Dyn.*, *21*, 689–698.

Larrasoaña, J. C., A. P. Roberts, J. S. Stoner, C. Richter, and R. Wehausen (2003b), A new proxy for bottom-water ventilation in the eastern Mediterranean based on diagenetically controlled magnetic properties of sapropel-bearing sediments, *Palaeogeogr. Palaeoclimatol. Palaeoecol.*, *190*, 221–242.

Liu, Q., S. K. Banerjee, M. J. Jackson, R. Zhu, and Y. Pan (2002), A new method in mineral magnetism for the separation of weak antiferromagnetic signal from a strong ferrimagnetic background, *Geophys. Res. Lett.*, *29*(12), 1565, doi:10.1029/2002GL014699.

Liu, Q., J. Torrent, Y. Yu, and C. Deng (2004), Mechanism of the parasitic remanence of aluminous goethite [$\alpha$-(Fe, Al)OOH], *J. Geophys. Res.*, *109*, B12106, doi:10.1029/2004JB003352.

Maher, B. A., and P. F. Dennis (2001), Evidence against dust-mediated control of glacial-interglacial changes in atmospheric $CO_2$, *Nature*, *411*, 176–180.

Mathé, P. E., P. Rochette, and D. Vandamme (1999), Néel temperature of synthetic substituted goethites and their rapid determination using low-field susceptibility curves, *Geophys. Res. Lett.*, *26*, 2125–2128.

Özdemir, Ö., and D. J. Dunlop (1996), Thermal remanence and Néel temperature of goethite, *Geophys. Res. Lett.*, *23*, 921–924.

Pollard, R. J., Q. A. Pankhurst, and P. Zientek (1991), Magnetism in aluminous goethite, *Phys. Chem. Miner.*, *18*, 259–264.

Roberts, A. P., Q. Liu, C. J. Rowan, L. Chang, C. Carvallo, J. Torrent, and C.-S. Horng (2006), Characterization of hematite ($\alpha$-$Fe_2O_3$), goethite ($\alpha$-FeOOH), greigite ($Fe_3S_4$), and pyrrhotite ($Fe_7S_8$) using first-order reversal curve diagrams, *J. Geophys. Res.*, *111*, B12S35, doi:10.1029/2006JB004715.

Robinson, S. G. (1986), The late Pleistocene palaeoclimatic record of North Atlantic deep-sea sediments revealed by mineral-magnetic measurements, *Phys. Earth Planet. Inter.*, *42*, 22–47.

Rochette, P., P.-E. Mathé, L. Esteban, H. Rakoto, J.-L. Bouchez, Q. Liu, and J. Torrent (2005), Non-saturation of the defect moment of goethite and fine-grained hematite up to 57 Teslas, *Geophys. Res. Lett.*, *32*, L22309, doi:10.1029/2005GL024196.

Scheinost, A. C., A. Chavernas, V. Barrón, and J. Torrent (1998), Use and limitations of second-derivative diffuse reflectance spectroscopy in the visible to near-infrared range to identify and quantify Fe oxide minerals in soils, *Clays Clay Miner.*, *46*, 528–536.

Schulze, D. G., and U. Schwertmann (1984), The influence of aluminum on iron oxides: X. Properties of Al-substituted goethites, *Clay Miner.*, *19*, 521–539.

Schulze, D. G., and U. Schwertmann (1987), The influence of aluminum on iron oxides: XII. Properties of goethites synthesized in 0.3 M KOH at 25°C, *Clay Miner.*, *22*, 83–92.

Schwertmann, U. (1988), Occurrence and formation of iron oxides in the various paleoenvironments, in *Iron in Soils and Clay Minerals*, edited by J. W. Stucki, B. A. Goodman, and U. Schwertmann, pp. 267–308, D. Reidel, Dordrecht, Netherlands.

Stancin, A. M., J. D. Gleason, D. K. Rea, R. M. Owen, T. C. Moore, Jr., J. D. Blum, and S. A. Hovan (2006), Radiogenic isotopic mapping of late Cenozoic eolian and hemipelagic sediment distribution in the east-central Pacific, *Earth Planet. Sci. Lett.*, *248*, 840–850.

Stokking, L., and L. Tauxe (1990), Multicomponent magnetization in synthetic hematite, *Phys. Earth Planet. Inter.*, *65*, 109–124.

Thompson, R., and F. Oldfield (1986), *Environmental Magnetism*, 229 pp., Allen and Unwin, London.

Torrent, J., U. Schwertmann, and D. G. Schulze (1980), Iron oxide mineralogy of some soils of two river terrace sequences in Spain, *Geoderma*, *25*, 191–208.

Torrent, J., U. Schwertmann, and V. Barrón (1987), The reductive dissolution of synthetic goethite and hematite in dithionite, *Clay Miner.*, *22*, 329–337.

Torrent, J., V. Barrón, and U. Schwertmann (1990), Phosphate adsorption and desorption by goethites differing in crystal morphology, *Soil Sci. Soc. Am. J.*, *54*, 1007–1012.

Verosub, K. L., and A. P. Roberts (1995), Environmental magnetism: Past, present, and future, *J. Geophys. Res.*, *100*, 2175–2192.

Weeks, R., C. Laj, L. Endignoux, M. Fuller, A. Roberts, R. Manganne, E. Blanchard, and W. Goree (1993), Improvements in long-core measurement techniques: Applications in palaeomagnetism and palaeoceanography, *Geophys. J. Int.*, *114*, 651–662.

Wells, M. A., R. W. Fitzpatrick, R. J. Gilkes, and J. Dobson (1999), Magnetic properties of metal-substituted haematite, *Geophys. J. Int.*, *138*, 571–580.

Yamazaki, T., and N. Ioka (1997), Environmental rock-magnetism of pelagic clay: Implications for Asian eolian input to the North Pacific since the Pliocene, *Paleoceanography*, *12*, 111–124.